Nanoscale

COMMUNICATION

View Article Online
View Journal

Cite this: DOI: 10.1039/c8nr07259k

Received 6th September 2018,
Accepted 25th November 2018

DOI: 10.1039/c8nr07259k

rsc.li/nanoscale

Tuning coiled coil stability with histidine-metal coordination†

Isabell Tunn, [a] Alberto S. de Léon, [a] Kerstin G. Blank *[a] and Matthew J. Harrington*[a,b]

Coiled coils (CCs) have emerged as versatile building blocks for the synthesis of nanostructures, drug delivery systems and biomimetic hydrogels. Bioengineering metal coordination sites into the terminal ends of a synthetic coiled coil (CC), we generate a nanoscale biological building block with tunable stability. The reversible coordination of Ni^{2+} thermodynamically stabilizes the CC, as shown with circular dichroism spectroscopy. Using atomic force microscopy-based single-molecule force spectroscopy, it is further shown that Ni^{2+}-binding reinforces the CC mechanically, increasing the barrier height for dissociation. When used as a dynamic cross-link in polyethyleneglycol-based hydrogels, the single-molecule stability of the CC is directly transferred to the bulk material and determines its viscoelastic properties. This reversibly tunable CC, thus, highlights an effective strategy for rationally engineering the single-molecule properties of biomolecular building blocks, which can be translated to the emergent properties of biomimetic materials, as well as other CC containing molecular assemblies.

Introduction

The supramolecular assembly of proteinaceous building blocks *via* non-covalent interactions is emerging as an effective strategy for producing biocompatible hydrogels[1] as well as nanoarchitectures with increased structural and functional complexity.[2,3] However, molecular control of their thermodynamic and mechanical stability remains a significant hurdle. Here, we employ a rational bottom-up approach towards bioengineering a tunable peptide building block. We combine two prominent material design paradigms found in natural supramolecular materials – namely, the coiled coil (CC) protein-folding motif and histidine (His)–metal cross-linking. The CC protein-folding motif is a common conformational feature of proteins with essential mechanical function in mammalian tissues (*e.g.* in molecular motors and extracellular matrix components)[1] and further appears as a frequent building block for many proteinaceous biological materials (*e.g.* in wool, hagfish slime and gastropod egg capsules).[7] CCs consist of two to seven α-helices wrapped around each other to form a superhelix.[1] The structure and conformation of CCs is determined by a specific repeat of seven amino acids (*abcdefg*), called a heptad. The overall stability of the CC superhelix originates from hydrophobic interactions at positions *a* and *d*, ionic interactions at positions *e* and *g*, as well as the stability of the individual α-helices, which can be tuned by including amino acids with different helix propensity[8] especially in the solvent-exposed positions *b*, *c* and *f*.

His–metal coordination bonds are strong, non-covalent interactions with self-healing properties, observed, for example, in mussel byssal threads and spider fangs.[9,10] Rationally engineering His–metal coordination sites into proteins has already been demonstrated to increase thermodynamic and mechanical stability.[11–14] Here, we introduce His–metal coordination sites into the sequence of a well-characterized synthetic heterodimeric CC (A_4B_4).[5,6] Considering that the terminal helical turns of CCs are more dynamic,[15] we therefore hypothesize that bridging these helical turns with metal coordination bonds (Fig. 1A) will have a stabilizing effect on the entire CC. To achieve this, we introduce His at the solvent exposed *b* and *f* positions of the terminal heptads of the CC (HA_4HB_4), spacing the His residues in a distance of *i*, *i* + 4 (Fig. 1B). This ensures a proper geometric configuration for forming chelate complexes with transition metals.[11,16] In addition to the expected thermodynamic stabilization, we further hypothesize that metal-coordinated helical turns will also affect the mechanical stability of CCs. Using molecular dynamics (MD) simulations, we have recently investigated the mechanistic response of a heterodimeric 4-heptad CC to an externally applied shear force. These simulations suggest that the applied force causes the consecutive

[a]*Max Planck Institute of Colloids and Interfaces, Science Park Potsdam-Golm, 14424 Potsdam, Germany. E-mail: Kerstin.Blank@mpikg.mpg.de*
[b]*McGill University, 801 Sherbrooke St West, Montreal, Quebec H3A 0B8, Canada. E-mail: Matt.Harrington@mcgill.ca*

† Electronic supplementary information (ESI) available: Methods and data of the Raman, CD, SMFS and rheology experiments. See DOI: 10.1039/c8nr07259k

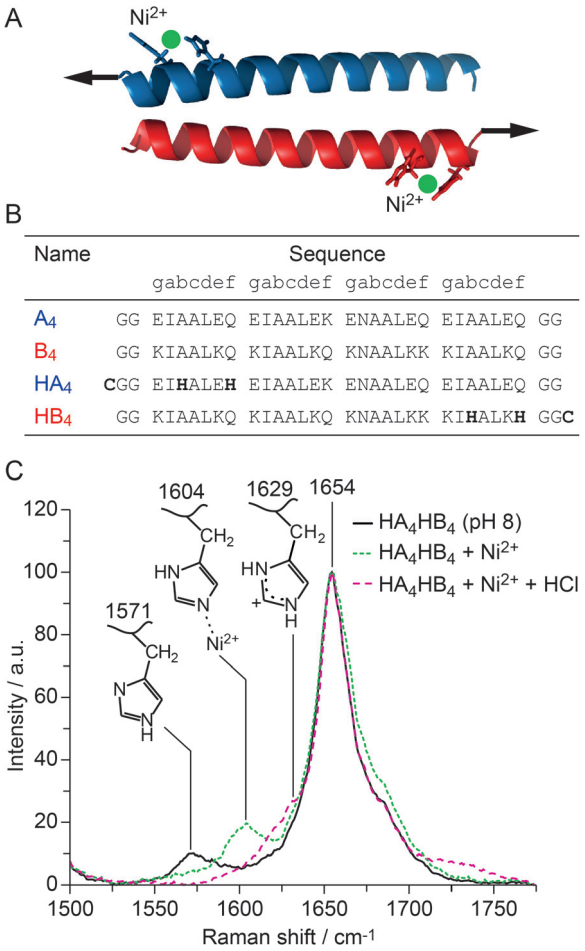

Fig. 1 Design and structural characterization of the His-modified CC. (A) Structural model of the CC generated with CC-builder,[4] showing the His–metal coordination bridges. Arrows indicate the direction and point of origin of the applied shear force. (B) Amino acid sequence of the reference peptides A_4 and B_4[5,6] as well as the His-modified peptides HA_4 and HB_4. The terminal cysteines serve for coupling the peptides to maleimide-functionalized PEG. They were absent in the peptides used for structural and thermodynamic characterization. (C) Raman spectra of thin films of HA_4HB_4 formed at pH 8 without metals, with 2 : 1 His : Ni^{2+}, and with Ni^{2+} at acidic pH.

unfolding of helical turns, most likely initiated at the termini where the force is applied.[6] Introducing His–metal bridges into the mechanically loaded heptads (Fig. 1A and B) is thus expected to stabilize the helices against mechanically induced unfolding, allowing us to experimentally test and verify the predicted mechanism. To investigate the possible effect of metal coordination, we focus on Ni^{2+} as the coordinating metal, since it has been shown to exhibit slow bond dynamics combined with rupture forces ranging from 40 pN to 300 pN.[17,18]

Results and discussion

Raman spectroscopy was used to investigate both the secondary structure of the CC (characteristic amide vibrational bands[19]) and the ability of His to coordinate Ni^{2+}. Histidine shows distinct vibrational modes that are extremely sensitive to the protonation and coordination state of its functional group.[20] The resulting Raman peaks, originating from $C_4{=}C_5$ vibrations of the imidazole ring, are expected in the range from 1550–1640 cm^{-1}. The Raman spectrum of HA_4HB_4 shows an amide I peak at 1654 cm^{-1}, confirming the α-helical secondary structure of the CC (Fig. 1C). The peak at 1571 cm^{-1} is assigned to deprotonated His at pH 8.0.[19,20] Upon addition of $NiCl_2$ in a ratio of 2 : 1 His : Ni^{2+}, the His peak shifts to 1604 cm^{-1} due to His–Ni^{2+} coordination. After acidifying the solution, the dominant peak at 1629 cm^{-1} indicates that His becomes protonated and no longer coordinates Ni^{2+}. This clearly reveals that the interaction between His and Ni^{2+} is reversible. HA_4HB_4 was further investigated using circular dichroism (CD) spectroscopy, which shows the expected spectrum with two minima at 208 nm and 222 nm, characteristic for an α-helical structure (Fig. S1A†). CD spectroscopy was also used to investigate the thermodynamic stability of the CC in the presence and the absence of $NiCl_2$, performing thermal unfolding experiments (Fig. S1B†). His–Ni^{2+} coordination (1 : 3 His : Ni^{2+} ratio) increased the melting temperature (T_m) of HA_4HB_4 from 76.4 ± 0.9 °C to 80.2 ± 0.6 °C. In contrast, no Ni^{2+}-induced stabilization was observed in the reference CC A_4B_4, which lacks His (Fig. 1B and Fig. S2†). A comparable thermodynamic stabilization induced by His–metal coordination was described previously for several other proteins.[11,21]

To obtain more detailed insight into the stabilizing effect of His–Ni^{2+} coordination, single-molecule force spectroscopy (SMFS) was performed. SMFS directly probes whether His–Ni^{2+} coordination mechanically stabilizes the CC and, more importantly, provides information about the effect of bridging the terminal helical turns on the energy landscape of the CC interaction. The two peptides HA_4 and HB_4 were immobilized separately, either to the AFM cantilever or to a glass surface (Fig. 2A). For this purpose, cysteine was introduced at the respective termini and the peptides were coupled to surfaces functionalized with maleimide-terminated polyethyleneglycol (PEG).[22] Fig. 2B shows typical force–distance curves recorded at a retract speed of 400 nm s^{-1} in the presence and absence of 1 mM $NiCl_2$. The resulting rupture force histograms show that His–Ni^{2+} coordination increases the rupture force of HA_4HB_4 by ~10 pN (Fig. S3†). Adding an excess of chelating agent, such as ethylenediaminetetraacetic acid (EDTA), reduces the rupture force by approximately the same value, supporting the observation that the stabilizing effect of His–Ni^{2+} coordination is fully reversible (Fig. 2B). This result is a first indication that the computationally proposed mechanism of mechanical CC unfolding is reproduced in our SMFS experiments and that the CC can be stabilized against shear forces when bridging the terminal helical turns at the points of force application.

To investigate the dynamic mechanical response of HA_4HB_4 and to understand how His–Ni^{2+} coordination affects the energy landscape of the CC, the measurements were repeated at different retract speeds and the most probable rupture

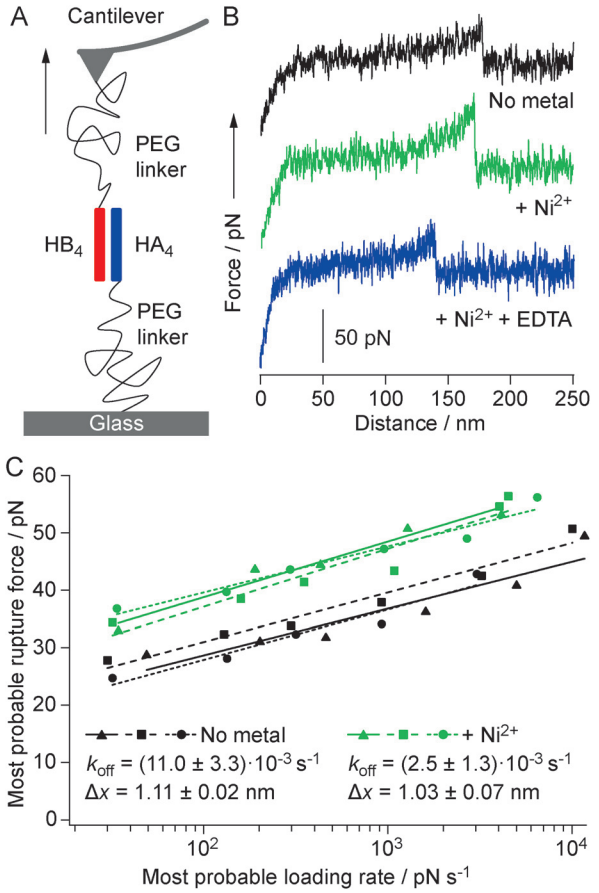

Fig. 2 Single-molecule force spectroscopy of HA_4HB_4. (A) Experimental setup. The individual CC-forming peptides were coupled to either the cantilever or the glass surface *via* a PEG linker. A maleimide-functionalized PEG was used for coupling the Cys-terminated peptides. (B) Typical force distance curves of the His-modified CC in the absence and presence of 1 mM Ni^{2+} and after washing with 10 mM EDTA. (C) Results of the dynamic SMFS measurements of the His-modified CC in the presence and absence of 1 mM Ni^{2+}. The most probable rupture forces were plotted *versus* the logarithm of the most probable loading rates. Three data sets (triangles, squares, circles) were obtained per condition, using three different cantilevers and surfaces. The lines are fits to the Bell–Evans model. The parameters k_{off} and Δx obtained from the fits to the single data sets are shown in Table S2.† The mean values ± SEM are reported in this figure.

forces (F_R) and the corresponding loading rates ($\dot{F}$) were determined (see Fig. S4, S5 and Table S1† for representative data sets obtained in the absence and the presence of 1 mM $NiCl_2$). Fig. 2C reveals a linear dependency of F_R on the logarithm of $\dot{F}$, which can be described with the Bell–Evans model (see ESI†).[23]

Fitting the data sets with the Bell–Evans equation yields the extrapolated thermal off-rate at zero force (k_{off}) and the potential width (Δx). Notably, the mean k_{off} in the presence of 1 mM Ni^{2+} (2.5×10^{-3} s^{-1}) is almost one order of magnitude lower than in the absence of 1 mM Ni^{2+} (11.0×10^{-3} s^{-1}), indicating that the barrier height to dissociation is increased when Ni^{2+} is bound (Fig. 2B). In contrast, the potential width Δx is not significantly different in the absence and presence of Ni^{2+} (Table S2†), suggesting that the mechanical dissociation pathway of the CC is not changed. Considering the proposed mechanism, this again confirms the stabilizing effect of the His–Ni^{2+} bridge. We propose that stabilization primarily affects the individual helices.[11,13,14] As a secondary effect, the reduced conformational freedom of one helix is transferred to the second helix *via* the hydrophobic core, thereby synergistically increasing the stability of the entire CC. This interpretation is supported by the observation that the presence of a third helix (CC trimer) greatly stabilizes the CC against shear forces.[24]

It remains an open question what exactly causes the increased energy barrier. It may originate from the simultaneous rupture of the His–Ni^{2+} bond and the helix stabilizing hydrogen bonds. Alternatively, the His–Ni^{2+} stabilized heptads may remain intact, forcing the CC to start uncoiling at internal heptads, which are stabilized by a larger number of hydrogen bonds. No information is available about the unbinding and rebinding kinetics of the His–Ni^{2+} bridge and the rupture forces reported for His : Ni^{2+} bonds lie in the range between 40 and 300 pN.[9] This force range overlaps with the rupture forces of the CC so that no direct conclusion is possible about which scenario is more likely. Additional experiments using an irreversible bridge, such as a covalent staple,[25,26] would be required to unambiguously answer this question. Despite this remaining question, the results show that His–Ni^{2+} coordination stabilizes HA_4HB_4 thermodynamically and mechanically and that our rational bottom-up approach is valid.

Based on the evidence above, the engineered CC has an excellent potential to be used as a building block for the synthesis of biomimetic materials and supramolecular assemblies with tunable stimuli-responsive behaviors. As a proof-of-concept demonstration that molecular level tunability can be translated into bulk-scale dynamic properties, we used HA_4HB_4 as a supramolecular crosslink for the production of polymer–peptide hybrid hydrogels. Cysteine-containing HA_4 and HB_4 were each separately coupled to maleimide-terminated star-shaped polyethyleneglycol (sPEG, 4 arms) and gels were formed by mixing the two in a stoichiometric ratio (Fig. 3 inset). Using oscillatory rheology, the viscoelastic properties of the CC-crosslinked hydrogel were investigated in the absence and presence of Ni^{2+} (ratio of 1 : 1 His : Ni^{2+}) and after adding 10 mM EDTA to the Ni^{2+}-containing hydrogel. Amplitude sweeps show a linear viscoelastic behavior up to at least 100% strain (Fig. S6†). At strains above 100% the storage modulus G' starts to decrease while the loss modulus G'' increases, indicating the onset of CC rupture. Due to the reversible nature of the CC crosslinks, the mechanical properties fully recover when the strain is lowered to 1% (Fig. S6†), indicating dynamic self-healing. Frequency sweeps performed at 1% strain (Fig. 3) give insights into this dynamic behavior. As described by the Maxwell model[27] for reversibly crosslinked networks, the relaxation time τ was obtained from the crossover frequency (ω_{CR}) of the G' and G'' curves of all three hydrogels. A comparison of τ shows that the addition of

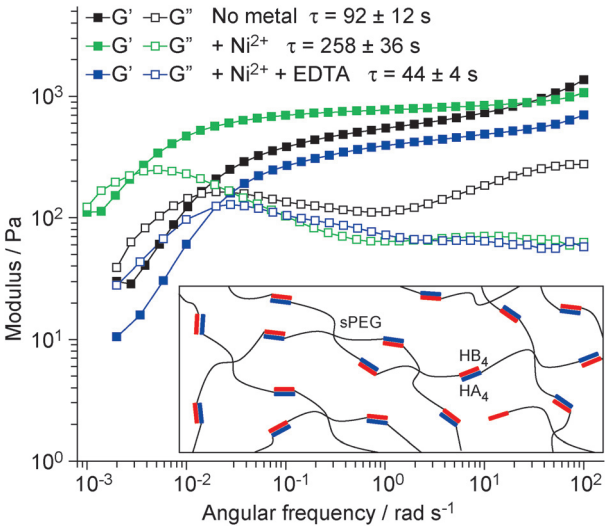

Fig. 3 Oscillatory shear rheology of HA_4HB_4-crosslinked sPEG hydrogels. Frequency sweep of the CC-crosslinked hydrogel at a constant strain amplitude of 1%, without metals, with 1 : 1 His : Ni^{2+} and 1 : 1 His : Ni^{2+} + EDTA (10 mM). G' is the storage modulus and G'' is the loss modulus. The crossover of G' and G'' (ω_{CR}) yields the relaxation time ($\omega_{CR} = 1/\tau$). Inset: Schematic representation of the hydrogel structure.

Ni^{2+} increases the mean relaxation time by ~3-fold from 92 ± 12 s to 258 ± 36 s – an effect that is fully reversed upon treatment with EDTA (τ = 44 ± 4 s). Notably, the relaxation time, which provides information about the average supramolecular lifetime of the CC crosslinks,[27] shows a similar trend as k_{off} determined with SMFS. Thus, it stands to reason that reducing k_{off} for single CC crosslinks *via* metal chelation, effectively increases the bond lifetime of the crosslink and shifts ω_{CR} to lower values. This direct correlation is additional proof for the functionality of the engineered CC building block and highlights that engineering the molecular parameters of hydrogel building blocks directly determines bulk material properties.

Conclusions

In summary, the presented rational design approach sheds new insights into the factors controlling CC stability. It allowed us to test and validate the prediction that bridging individual helical turns stabilizes the entire CC, thermodynamically and mechanically. These important mechanistic insights enabled us to reversibly tune the stability of the CC and provide a proof-of-concept demonstration of the potential of this versatile nanomechanical building block for biomimetic materials. Specifically, when used as a hydrogel crosslink, the CC molecular properties directly determine the performance of the bulk material in a metal-dependent manner. This provides a solid starting point for the development of a library of tunable CC building blocks with the potential of synthesizing well-controlled and dynamic hydrogels. Future studies will focus on expanding the tunable range, repositioning the stabilizing bridge to other heptads or using other transition metal ions, such as Cu^{2+}, Co^{2+} and Zn^{2+} as well as covalent staples.[27]

Conflicts of interest

There are no conflicts to declare.

Acknowledgements

The project was financially supported by the Max Planck Society and the International Max Planck Research School (IMPRS) on Multiscale Bio-Systems. ASL acknowledges support from a postdoctoral fellowship of the Alexander von Humboldt Foundation. Open Access funding provided by the Max Planck Society.

Notes and references

1 B. Apostolovic, M. Danial and H.-A. Klok, *Chem. Soc. Rev.*, 2010, **39**, 3541.
2 G. C. Pugh, J. R. Burns and S. Howorka, *Nat. Rev. Chem.*, 2018, **2**, 113.
3 A. Ljubetič, I. Drobnak, H. Gradišar and R. Jerala, *Chem. Commun.*, 2016, **52**, 5220.
4 C. W. Wood, M. Bruning, A. Á. Ibarra, G. J. Bartlett, A. R. Thomson, R. B. Sessions, R. L. Brady and D. N. Woolfson, *Bioinformatics*, 2014, **30**, 3029.
5 F. Thomas, A. L. Boyle, A. J. Burton and D. N. Woolfson, *J. Am. Chem. Soc.*, 2013, **135**, 5161.
6 M. Goktas, C. Luo, R. M. A. Sullan, A. E. Bergues-Pupo, R. Lipowsky, A. Vila Verde and K. G. Blank, *Chem. Sci.*, 2018, **9**, 4610.
7 A. Miserez and P. A. Guerette, *Chem. Soc. Rev.*, 2013, **42**, 1973.
8 J. R. Litowski and R. S. Hodges, *J. Biol. Chem.*, 2002, **277**, 37272.
9 E. Degtyar, M. J. Harrington, Y. Politi and P. Fratzl, *Angew. Chem., Int. Ed.*, 2014, **53**, 12026.
10 C. N. Z. Schmitt, Y. Politi, A. Reinecke and M. J. Harrington, *Biomacromolecules*, 2015, **16**, 2852.
11 F. H. Arnold and B. L. Haymore, *Science*, 1991, **252**, 1796.
12 Y. Cao, T. Yoo and H. Li, *Proc. Natl. Acad. Sci. U. S. A.*, 2008, **105**, 11152.
13 W. D. Kohn, C. M. Kay, B. D. Sykes and R. S. Hodges, *J. Am. Chem. Soc.*, 1998, **120**, 1124.
14 T. Miura, T. Satoh and H. Takeuchi, *Biochim. Biophys. Acta*, 1998, **1384**, 171.
15 G. De Crescenzo, J. R. Litowski, R. S. Hodges and M. D. O'Connor-McCourt, *Biochemistry*, 2003, **42**, 1754.
16 S. Knecht, D. Ricklin, A. N. Eberle and B. Ernst, *J. Mol. Recognit.*, 2009, **22**, 270.
17 M. Conti, G. Falini and B. Samorì, *Angew. Chem., Int. Ed.*, 2000, **39**, 215.

18 L. Schmitt, M. Ludwig, H. E. Gaub and R. Tampé, *Biophys. J.*, 2000, **78**, 3275.
19 Z. Movasaghi, S. Rehman and D. I. U. Rehman, *Appl. Spectrosc. Rev.*, 2007, **42**, 493.
20 H. Takeuchi, *Biopolymers*, 2003, **72**, 305.
21 M. R. Ghadiri and C. Choi, *J. Am. Chem. Soc.*, 1990, **112**, 1630.
22 J. L. Zimmermann, T. Nicolaus, G. Neuert and K. Blank, *Nat. Protoc.*, 2010, **5**, 975.
23 E. Evans, *Annu. Rev. Biophys. Biomol. Struct.*, 2001, **30**, 105.
24 A. E. Bergues-Pupo, K. G. Blank, R. Lipowsky and A. Vila Verde, *Phys. Chem. Chem. Phys.*, 2018, DOI: 10.1039/c8cp04896g.
25 Y.-W. Kim and G. L. Verdine, *Bioorg. Med. Chem. Lett.*, 2009, **19**, 2533.
26 G. L. Verdine and G. J. Hilinski, *Methods Enzymol.*, 2012, **503**, 3.
27 S. C. Grindy, R. Learsch, D. Mozhdehi, J. Cheng, D. G. Barrett, Z. Guan, P. B. Messersmith and N. Holten-Andersen, *Nat. Mater.*, 2015, **14**, 1210.